

Designing the Waveform Bandwidth and Time Duration of Automotive Radars for Better Collision Warning Performance

Hang Ruan, Yimin Liu, *Member, IEEE*, Tianyao Huang, and Xiqin Wang

Automotive radar is a key component in an advanced driver-assistance system (ADAS). The increasing number of radars implemented in vehicles makes interference between them a noteworthy issue. One method of interference mitigation is to limit the time-bandwidth product (TBP) of radar waveforms. However, the problems of how much TBP is necessary and how to optimally utilize the limited TBP have not been addressed. We take collision warning system (CWS) as an example and propose a method of designing the radar waveform parameters oriented by the performance of CWS. We propose a metric to quantify the CWS performance and study how the radar waveform parameters (bandwidth and duration) influence this metric. Then, the waveform parameters are designed with a limit on the TBP to optimize the system performance. Numerical results show that the proposed design outperforms the state-of-the-art parameter settings in terms of system performance and resource or energy efficiency.

Index Terms—Automotive radar, interference mitigation, collision warning system, time-bandwidth product

I. INTRODUCTION

An ADAS is designed to promote quality of driving experience, including safety, comfort and fuel economy [1]. There are different types of ADAS with varying purposes. Collision warning/collision avoidance (CW/CA) systems aim to detect potential collisions with objects in front of the vehicle and take corresponding actions, and adaptive cruise control (ACC) systems focus on speed and distance control in the car-following process [2]. For such systems to work, a vehicle is equipped with sensors to obtain information from its surrounding. Automotive radar plays an indispensable role among these sensors due to its high measurement accuracy, long detection range and robustness in different weather situations [3].

A radar measures the range and velocity of object in the front, which are two essential inputs for an ADAS. In a CWS, indices, such as time-to-collision (TTC) and warning distance, are calculated with these inputs and the system decides whether to give a warning accordingly [4]. In an ACC system, a control is generated based on the measurements [5].

The range and velocity are measured by estimating the delay and Doppler shift of the received signal [6]. Besides high signal-to-noise ratio (SNR), there are requirements on the bandwidth and duration of radar waveform to obtain accurate

estimates. The delay can be obtained through pulse compression and high accuracy of delay requires great bandwidth of the waveform. The Doppler shift can be obtained through coherent processing of a pulse sequence and high accuracy of velocity requires long duration of the waveform [6].

To ensure the performance of an ADAS, one essential radar requirement is to obtain accurate measurements. As introduced above, range measurement with high resolution and accuracy demands a wide spectrum, while velocity measurement demands a long duration [7]. In other words, a radar requires adequate electromagnetic resources in both the frequency and time domains to obtain reliable measurements. With the popularization of automotive radars, however, it will be common that multiple radars operate at the same time and in the same neighborhood [8]. The wider spectrum and longer duration of a single radar waveforms will result in a greater possibility of spectral conflict between radars, resulting in issues such as an increased noise floor and ghost targets [9], [10]. These problems degrade radar's performance in estimation and detection and this further leads to performance degradation of the ADAS. Therefore, countermeasures have to be implemented to mitigate interference, which can be classified into the following two schemes shown in Fig. 1:

- 1) Overlapped sharing scheme: The entire electromagnetic resources, in the frequency and time domains, are divided into several subsets. Each subset contains part of the whole bandwidth and time slots with no mutual overlap. Each radar uses some of the subsets according to a certain strategy. In this case, spectral conflict is likely to occur due to lack of coordination. Metrics such as outage probability are studied to evaluate the scheme [11], [12]. The interference can be further mitigated by implementing interference cancellation, beamforming and polarization [8], [9], [13]. These techniques, however, increase the signal processing complexity, increase the hardware cost [14] and achieve only limited SINR improvement [8].
- 2) Non-overlapped allocation scheme: Centralized control is assumed to be feasible in this scheme (such control may be realized through vehicle-to-vehicle (V2V) and vehicle-to-infrastructure (V2I) communications [15]), and the entire resources (in the frequency and time domains) are allocated to radars in a conflict-free way according to individual demands [16]–[19]. Ideally, spectral interference can be suppressed or even avoided. For example, [17] proposes a mechanism called RadarMAC, in which a control center collects the positions and trajectories of vehicles in some region first and then

H. Ruan, Y. Liu, T. Huang and X. Wang are with the Department of Electronic Engineering, Tsinghua University, Beijing, 100084 China (email: ruanh15@mails.tsinghua.edu.cn; yiminliu@tsinghua.edu.cn; huang-tianyao@tsinghua.edu.cn; wangxq_ee@tsinghua.edu.cn). Y. Liu is the corresponding author.

This work was supported by the National Natural Science Foundation of China (Grant No. 61801258).

Some preliminary results of this work were submitted the IEEE Radar Conference 2020.

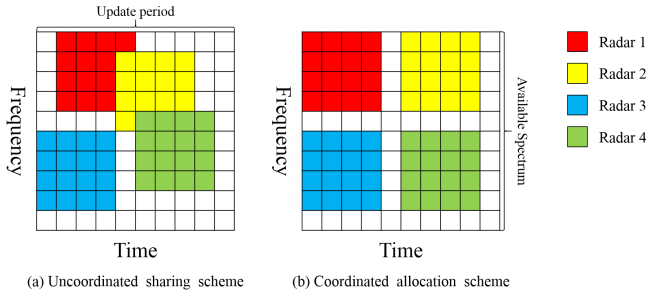


Fig. 1. A sketch of (a) the uncoordinated sharing scheme and (b) the coordinated allocation scheme. In the coordinated scheme, guard intervals are reserved in both the time and frequency domains to avoid signal overlap due to time delay and Doppler shift, respectively.

allocate the resources to vehicles without overlap.

For both sharing and allocation schemes, the TBP of the radar waveform is a key parameter since it quantifies how many resources in the frequency and time domains are occupied by the radar. For the sharing scheme, greater TBP occupied by one radar leads to a greater probability of spectral conflict [11], [12], while for allocation, greater TBP occupied leads to fewer radars that can operate in the same place and at the same time without interference [17], [18]. Therefore, the interference problem can be mitigated if the TBP of radar waveform is as small as possible, or in other words, the radar occupies as few electromagnetic resources as possible. This result motivates us to take resource efficiency into consideration when designing radar waveform.

Generally speaking, the existing studies on radar waveform design can be classified into waveform parameter design and baseband waveform design. As for waveform parameter design, parameters are designed to meet certain requirements on radar performance. One typical example is that requirements on measuring (e.g., range and velocity resolution) are proposed and the corresponding parameters (e.g., bandwidth and duration) are designed accordingly [20]–[23]. As for baseband waveform design, the frequency modulated continuous wave (FMCW) is widely used in due to its low transmit power [24], [25], while the orthogonal frequency division multiplexing (OFDM) is another alternative due to its flexibility in waveform optimization and convenience in integration with communication systems [26], [27]. The baseband waveform can be further optimized to improve radar’s performance. Metrics, including mutual information [28], [29] and Cramer-Rao lower bound (CRLB) [27], [30] are used for evaluating radar’s performance in the optimization problems. The ambiguity function is also used for optimization since it affects radar’s range and velocity resolution [31], [32].

Moreover, when the electromagnetic resources occupied by a radar, quantified by TBP, are limited, there is a tradeoff of estimation accuracy between range and velocity. Authors in [30], [33] express the tradeoff through multiplying the CRLB of range and velocity by a weighting matrix. The authors in [30] further explore the Pareto-optimal region of delay-Doppler estimation by changing the weighting matrix. However, the tradeoff in [30] is made with a limited on the transmit power instead of TBP. Moreover, it is not addressed how to

design the weighting matrix and find an optimal tradeoff. In this respect, the relationship between radar performance and system performance expresses one way of tradeoff. The main purpose of our paper is to express the tradeoff in terms of system and to design the waveform by finding the optimum of tradeoff.

To summarize, many existing studies on waveform design are targeted to specific radar performances, meaning that they consider the radar as a separated sensor from the ADAS. They do not jointly consider how the radar performance influences the system performance. Therefore, the electromagnetic resources are not fully exploited in terms of system performance. When the issue of interference among automotive radars becomes increasingly severe, however, it is necessary for the radars to utilize the limited resources more efficiently. Understanding the relationship between radar performance and system performance is a key to improving the efficiency.

Based on the above discussion, we propose a novel method of designing radar waveform parameters oriented to the performance of CWS. We evaluate the system performance by introducing the minimal total wrong decision loss (MTWDL) as the metric, which quantifies the costs of the system when a warning is triggered wrongly in a safe case or is not triggered timely in a dangerous situation. We then analyze the relationship between this metric and radar parameters (bandwidth and duration), based on which waveform parameters are designed through minimizing the MTWDL of the system under the TBP constraint. Compared with the existing design method, our method enables the radar to use fewer electromagnetic resources while guaranteeing the CWS to function normally. The main contributions of this paper are as follows:

- 1) We introduce MTWDL as the performance metric of CWS and analyze its relationship with radar performance. Analysis reveals that the system performance relies on what we defined as range-velocity joint error index (called error index for short), which is a weighted sum of variances of range and velocity estimation. This result indicates that in order to improve the performance of CWS, we should minimize the error index, yielding the waveform design criterion.
- 2) Using the above criterion, we propose a method optimizing the waveform parameters under the constraint of TBP, which limits the resources consumed by radar. Both theoretical and numerical results show that our optimized parameter design outperforms the state-of-art-design in terms of system performance, resource efficiency and energy efficiency.
- 3) To quantify the relationship between system performance and waveform parameters, we evaluate the estimation error of radar. To this end, we derive asymptotic the CRLB of range and velocity estimation using the FMCW in a multi-target scenario.

In summary, the proposed method raises waveform design to the level of the system that radar serves. By mining the relationship between system performance and waveform parameters, this method enables the radar to utilize the limited electromagnetic resources more efficiently and has the

potential to mitigate the tense resources. Our methodology can be applied to waveform design of radar in other systems, especially those also facing the problem of resource shortage.

The remainder of this paper is arranged as follows: In Section II, we formulate the signal model, derive CRLB of range and velocity and study the distribution of estimation errors. In Section III, we specify the collision warning system in this study, including its hypothesis, decision rule and derive the performance metric. In Section IV, we propose a method of waveform parameter design to optimize the system performance. The numerical results are shown in Section V. Section VI presents the conclusion and outlook.

II. SYSTEM AND SIGNAL MODEL

The procedure of a radar-based CWS can be divided into three steps: detecting object, estimating parameters and making decisions [34], as shown in Fig. 2. More detailed explanations are given as follows:

- 1) Object detection: The system tells whether there is an object in the front according to the received signal of radar. A common method is to compare the amplitude of signal after matched filtering (MF) with a certain threshold [35]. If the amplitude is larger than the threshold, the system tells that an object is detected. The performance of object detection mainly depends on the SNR.
- 2) Parameter estimation: If an object in the front is detected, the system estimate parameters of this object, e.g., range and relative velocity, with the received signal. Maximum likelihood estimation (MLE) is usually used for this purpose. The bandwidth and duration of waveform influence the accuracy of measurements.
- 3) Decision making: Based on the parameter estimates, the system decides whether the current situation is safe (negative hypothesis \mathcal{H}_0) or threatening (positive hypothesis \mathcal{H}_1) following a decision rule. If the situation is decided to be threatening (\mathcal{H}_1), the system will give a warning to the driver and the driver can response (e.g., brake) accordingly. Otherwise (\mathcal{H}_0), the system will not intervene on the driver's behaviour. The rule of making decisions will be discussed in Section III.

In this paper, we assume that an object is already detected in the front and focus on the second and third step. These two steps are analyzed in this section and Section III, respectively.

Our purpose is to design waveform parameters that optimize CWS performance, which relies on the distribution of radar's estimation errors. Therefore, we study the error distribution using the following steps: First, we present the signal model of an FMCW radar in Section II-A. Then, we derive the CRLB for range and velocity estimation in Section II-B, which facilitates the analysis on the error distribution in Section II-C.

A. Signal model

We analyze an FMCW radar using linear modulation. It is assumed that the radars are operating in the non-overlapped coordination scheme, so no interference exists among them.

The FMCW waveform is divided into M chirps and the pulse repetition interval (PRI) is T_0 , resulting in the duration as

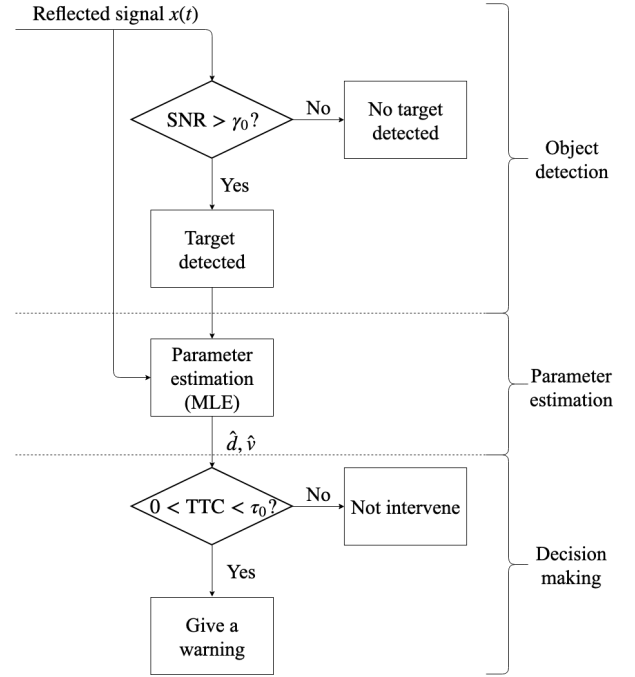


Fig. 2. A diagram of a radar-based CWS. The two dashed lines partition the three steps: object detection, parameter estimation and decision making.

$T = MT_0$. Within each chirp, the frequency of the waveform sweeps linearly from the initial frequency f_0 to $f_0 + W$, where W is the waveform bandwidth. We define the chirp rate as $\kappa = W/T_0$ and the amplitude is a real number A . Thus, the m -th ($m = 0, 1, \dots, M - 1$) chirp can be written as

$$s_m(t) = Ae^{j2\pi(f_0 t_m + \frac{1}{2}\kappa t_m^2)}, mT_0 \leq t < (m+1)T_0, \quad (1)$$

where we define $t_m = t - (m-1)T_0$.

The transmitted waveform is reflected by K scatterers. The echo from the k -th ($k = 1, 2, \dots, K$) scatterer is [36]

$$x_{k,m}(t) = \alpha_k s_m(t - 2(d_k + v_k t)/c), \quad (2)$$

where d_k and v_k are the range and relative velocity of the k -th scatterer, and α_k is the complex reflection intensity. The speed of light is denoted by c . The received signal within the m -th chirp, $x_m(t)$, is the sum of K echoes and noise, i.e.,

$$x_m(t) = \sum_{k=1}^K x_{k,m}(t) + w_m(t), \quad (3)$$

where $w_m(t)$ is the additive white Gaussian noise with power spectral density of N_0 . Note that the clutter is a key component in automotive radars. It is generated by the reflection of road surfaces and man-made structures on roads and can be treated as several stationary scatterers [37], meaning that it is included into the multi-scatterer signal model (3).

Upon mixing $x_m(t)$ with a local oscillator signal $s_{m,0}(t) = s_m(t)/A$ and low-pass filtering, the intermediate frequency (IF) signal $y_m(t)$ is obtained. With narrow-band and low-velocity assumption, the IF signal can be written as [36]

$$y_m(t) = \sum_{k=1}^K A\alpha_k^* e^{j\phi_k} e^{j2\pi f_{v,k} T_0 m + (f_{d,k} + f_{v,k})t_m} + w'_m(t). \quad (4)$$

The beat frequency $f_{d,k}$ and the Doppler shift $f_{v,k}$ are

$$f_{d,k} = 2\kappa d_k/c, f_{v,k} = 2f_0 v_k/c. \quad (5)$$

The phase $\phi_k = 4\pi f_0 d_k/c$ is time-invariant. The operator $*$ yields the complex conjugate of a number. The noise becomes $w'_m(t) = s_{m,0}(t)w_m^*(t)$. The IF signal $y_m(t)$ is then sampled at rate f_s , yielding the discrete-time signal as follows:

$$y[n,m] = \sum_{k=1}^K A\alpha_k^* e^{j\phi_k} e^{j2\pi(f_{v,k}T_0 m + (f_{d,k} + f_{v,k})n/f_s)} + w'[n,m], \quad (6)$$

where $n = 0, 1, \dots, N-1$ denotes the fast-time index. The total number of samples within one chirp is $N = f_s T_0$. Here, we assume that $f_s T_0$ is an integer. The variance of the noise $w'[n,m]$ is $\sigma_w^2 = f_s N_0$. The following manipulations are conducted on (6): The coefficients are merged as $A'_k = A\alpha_k^* e^{j\phi_k}$. We use b_k and ψ_k to denote the amplitude and phase of A'_k , i.e., $A'_k = b_k e^{j\psi_k}$. We define the two-dimensional frequencies

$$f_{1,k} = (f_{d,k} + f_{v,k})/f_s, f_{2,k} = f_{v,k}T_0. \quad (7)$$

Thus, the samples shown in (6) can be rewritten as

$$y[n,m] = \sum_{k=1}^K b_k e^{j\psi_k} e^{j2\pi(f_{1,k}n + f_{2,k}m)} + w'[n,m]. \quad (8)$$

The deterministic parameters to be estimated are formulated as $\xi = [\xi_1^T, \xi_2^T, \dots, \xi_K^T]^T$, where $\xi_k = [b_k, \psi_k, f_{1,k}, f_{2,k}]^T$. Here, the operator T yields the transpose of a matrix. After ξ is estimated, we further obtain the estimate of $\theta_k = [d_k, v_k]^T$ according to (5) and (7). Note that although ϕ_k contains the range d_k , it cannot be used to estimate d_k since the complex reflection intensity α_k also introduces an unknown phase, which cannot be separated from ϕ_k . Thus, we use the frequencies $f_{1,k}$ and $f_{2,k}$ to estimate θ_k .

As addressed in the beginning of this section, one common method of estimating θ_k is MLE. The process of MLE is as follows: we first conduct two-dimensional fast Fourier transform [38] on $y[n,m]$ and conduct detection in all the resolution cells. For each resolution cell that a target (numbered as k) is detected, we search the frequencies $\hat{f}_{1,k}$ and $\hat{f}_{2,k}$ within this cell such that the following expression

$$\left| \sum_{n=0}^{N-1} \sum_{m=0}^{M-1} y[n,m] e^{-j2\pi(\hat{f}_{1,k}n + \hat{f}_{2,k}m)} \right| \quad (9)$$

reaches its maximum. The corresponding $\hat{f}_{1,k}$ and $\hat{f}_{2,k}$ are the estimate of two-dimensional frequencies. Estimate of range and velocity, \hat{d}_k and \hat{v}_k , is obtained based on their relationship with the two frequencies given by (5) and (7).

B. CRLB for range and velocity estimation

Due to the existence of noise, estimation error is inevitable. Thus, the estimate can be written as

$$\hat{\theta}_k = \theta_k + \varepsilon_k, \quad (10)$$

where $\hat{\theta}_k = [\hat{d}_k, \hat{v}_k]^T$ denotes the estimate of range and velocity, and $\varepsilon_k = [\varepsilon_{d,k}, \varepsilon_{v,k}]^T$ denotes the error. The CRLB expresses a lower bound on the variance of unbiased estimators of a parameter [35] and we use it to evaluate the estimation error. The CRLB for θ_k is presented as follows:

Proposition 1. When M and N are sufficiently large, errors of estimating θ_k for different k are asymptotically uncorrelated and the CRLB for estimating θ_k can be approximated as

$$\mathbf{B}_{\theta,k} = \frac{3c^2}{8\pi^2\gamma_k} \text{diag} \left(\frac{1}{W^2}, \frac{1}{f_0^2 T^2} \right), \quad (11)$$

where $\gamma_k = |\alpha_k|^2 A^2 T / N_0$ is the SNR after MF.

Proof. See Appendix A. \square

We use $B_{d,k}$ and $B_{v,k}$ to denote the CRLBs, i.e.,

$$B_{d,k} = \frac{3c^2}{8\pi^2\gamma_k} \frac{1}{W^2}, B_{v,k} = \frac{3c^2}{8\pi^2\gamma_k} \frac{1}{f_0^2 T^2}. \quad (12)$$

When designing W and T , we assume that the SNR γ_k is a constant to fix the mean power of radar. The results in (12) illustrate that when γ_k is fixed, the CRLBs of d_k and v_k are inversely proportional to W^2 and T^2 , respectively. This implies that the accuracy of range and velocity measurement requires resources in the frequency time domain, respectively.

Moreover, although multiple scatterers are observed, we can consider that only one of them is critical for the system to decide whether to give a warning or not. We select the critical scatterer with the smallest positive TTC, since the CWS depends on such a scatterer to decide whether to warn or not, as shown in Section III. In the remainder, we assume that this scatterer is already selected and the subscript k is omitted for conciseness, e.g., $B_d = B_{d,k}$.

In conventional design of radar waveform, the bandwidth and duration are designed according to requirement on resolution of range and velocity, respectively. Their designs are separate. Nevertheless, when the waveform TBP is limited to restrict resource occupation, (12) implies that there is a tradeoff of accuracy between range and velocity. Our main purpose is to design the bandwidth and duration jointly to reach a tradeoff where the CWS achieves its best performance.

C. Distribution of estimation errors

We are now ready to derive the distribution of ε , as required for analysis on CWS performance. As stated in [35, Theorem 7.3], when the SNR is sufficiently high, the estimation error using MLE is asymptotically distributed (for large M and N) as a zero-mean Gaussian variable whose covariance is the CLRb. Thus, we assume that ε follows zero-mean Gaussian distribution with covariance $\Sigma_\varepsilon = \text{diag}(\sigma_d^2, \sigma_v^2)$, where

$$\sigma_d^2 = B_d = \frac{3c^2}{8\pi^2\gamma} \frac{1}{W^2}, \sigma_v^2 = B_v = \frac{3c^2}{8\pi^2\gamma} \frac{1}{f_0^2 T^2}. \quad (13)$$

To test this assumption, we generate observations according to (6) and use MLE to get samples of estimates. Two results are drawn from these samples: First, when the SNR is greater than 10 dB, which is a common case in practice [25], the covariance of range and velocity errors is close to their CRLB; Second, we conduct the Kolmogorov-Smirnov test [39] on samples of ε_d and ε_v , and the results do not reject the null hypothesis that the samples are drawn from the assumed Gaussian distribution at the 5% significance level, which verifies that the error follows a Gaussian distribution. The above results construct a preliminary verification about our assumption. It will be further checked through simulations in Section V.

III. PERFORMANCE OF COLLISION WARNING SYSTEM

After the range and velocity are estimated, the CWS decides whether the current situation is safe or threatening using a certain rule and takes corresponding actions. In this step, estimation errors of radar may lead to wrong decisions, which can be divided into two types: The first is triggering an alarm in a safe situation, i.e., deciding \mathcal{H}_0 as \mathcal{H}_1 , called a false alarm; The second regards a threatening case as safe, i.e., deciding \mathcal{H}_1 as \mathcal{H}_0 , called a miss [35]. In a CWS, we hope to reduce both false alarm and miss. However, when the radar performance is fixed, there is a tradeoff between these two types of wrong decisions [40]. Therefore, we propose total wrong decision loss (TWDL) that balances wrong decisions under all possible situations and further propose MTWDL as the performance metric of CWS based on TWDL. Then, we establish the relationship between the CWS performance metric and radar performance.

The remainder is arranged as follows: First, we set a criterion to partition \mathcal{H}_0 and \mathcal{H}_1 as well as test statistics in Section III-A. Second, we introduce TWDL as the performance metric of decision rule in Section III-B. Third, we further introduce MTWDL as the performance metric of CWS and analyze its relationship with radar performance in Section III-C.

A. Two hypotheses and test statistics

First, we need a criterion to partition safe and threatening situations (also called \mathcal{H}_0 and \mathcal{H}_1 hypothesis) based on the ground truth θ [4], [40]. Later, we will extend to the case when the ground truth is unknown. In this respect, the TTC is proven effective for partition [40], [41] and it is widely used in real systems [42], [43]. The TTC is defined as $\tau = -d/v$. Based on the TTC, hypotheses \mathcal{H}_1 and \mathcal{H}_0 are given by [40]

$$\begin{aligned} \mathcal{H}_1 : 0 < \tau < \tau_0, \\ \mathcal{H}_0 : \text{else.} \end{aligned} \quad (14)$$

That is, a threatening situation occurs when the vehicle is approaching some object and the TTC is less than a threshold τ_0 . Typical values of τ_0 are from three to five seconds in application [41]. Additionally, an equivalent form of (14) is

$$\begin{aligned} \mathcal{H}_1 : d + \tau_0 v < 0, \\ \mathcal{H}_0 : d + \tau_0 v \geq 0. \end{aligned} \quad (15)$$

In practice, the real value of θ cannot be known exactly due to the noise. The CWS makes a decision with the estimate $\hat{\theta} = [\hat{d}, \hat{v}]^T$, which contains error ε . One common method for decision with unknown parameters is the generalized likelihood ratio test (GLRT), which usually performs well [44]. According to Appendix B, the GLRT rule for the CWS is

$$T_G(\hat{\theta}) \underset{\mathcal{H}_1}{\overset{\mathcal{H}_0}{\geq}} \lambda, \quad (16)$$

where the test statistic is

$$T_G(\hat{\theta}) = \begin{cases} \hat{d} + \tau_0 \hat{v}, & \hat{d} > 0, \hat{d} \geq \frac{\sigma_d^2}{\sigma_v^2 \tau_0} \hat{v}, \\ \sqrt{\sigma_d^2 + \tau_0^2 \sigma_v^2} \sqrt{\frac{\hat{d}^2}{\sigma_d^2} + \frac{\hat{v}^2}{\sigma_v^2}}, & \hat{d} > 0, \hat{d} < \frac{\sigma_d^2}{\sigma_v^2 \tau_0} \hat{v}. \end{cases} \quad (17)$$

According to (17), there are two expressions of the test statistic $T_G(\hat{\theta})$ depending on the region that $\hat{\theta}$ lies in. For the simplicity of analysis, we also consider a test statistic using the first expression appearing in $T_G(\hat{\theta})$, given by

$$T_A(\hat{\theta}) = \hat{d} + \tau_0 \hat{v}. \quad (18)$$

Here, we make an explanation on why we construct the new statistic with the first expression in (17). According to (15), $d + \tau_0 v = 0$ is the boundary between safe and threatening situations. An intuition is that a situation with estimation $\hat{\theta} = [\hat{d}, \hat{v}]^T$ lying near the boundary has high potential of making a wrong decision and such situations are critical for the performance of CWS. Most of these critical points $\hat{\theta}$ lie in the first region shown in (17) and the approximate test statistic $T_A(\hat{\theta})$ equals $T_G(\hat{\theta})$ for these points. Moreover, for the critical points that lie in the second region shown in (17), the difference between $T_A(\hat{\theta})$ and $T_G(\hat{\theta})$ is small. Therefore, $T_A(\hat{\theta})$ can be a good approximate for $T_G(\hat{\theta})$. This will be further verified through numerical results in Section V.

We use $T_A(\hat{\theta})$ to make decisions with the following rule:

$$T_A(\hat{\theta}) \underset{\mathcal{H}_1}{\overset{\mathcal{H}_0}{\geq}} \lambda, \quad (19)$$

In the remainder, we call (16) the GLRT rule and call (19) the approximate rule. Both rules depend on a threshold λ . It is a tunable variable and selected to optimize the decision rule. For this purpose, we introduce a performance metric for decision rules in Section III-B, which enables us to find the optimal λ .

B. Performance metric of decision rule

Since the ground truth θ is unknown to the CWS, wrong decisions happen using a decision rule. In order to evaluate the performance of a decision rule, we introduce a metric called TWDL, which we describe in the following.

For a given pair of true values d and v , we use $P_w(d, v)$ to denote the probability of making a wrong decision, which depends on two hypotheses (15), decision rule and error distribution. Moreover, we use point wrong decision loss (PWDL), denoted by $u(d, v)$, to quantify the loss of a wrong decision. It is manually designed to reflect the severity of a wrong decision under different situations. The PWDL is a function of d and v , and is irrelevant of radar performance and decision rule, meaning that $u(d, v)$ is irrelevant of the decision threshold λ and the estimation error variances σ_d^2 and σ_v^2 . We integrate the product of $P_w(d, v)$ and $u(d, v)$ over a domain D , which contains all possible pairs of d and v in practice. The integral is the defined TWDL, given by

$$U = \iint_D u(d, v) P_w(d, v) ddv. \quad (20)$$

Through integration, the TWDL synthesizes wrong decisions under all situations within D and balances them according to respective probability and loss, i.e., $P_w(d, v)$ and $u(d, v)$. The TWDL is used to quantify the performance of a decision rule.

Moreover, simulations in Section V-B will show that the performance of the GLRT and approximate rules is pretty close. Our following theoretical analysis on the system performance is based on the approximate rule for simplicity.

With the hypotheses (15) and approximate decision rule (19), we derive the probability $P_w(d, v)$ analytically. For instance, when $d + \tau_0 v$ is non-negative, representing a safe situation \mathcal{H}_0 , $P_w(d, v)$ is the probability that a warning is given according to the rule (19) with estimate $\hat{\theta} = [\hat{d}, \hat{v}]^T$. Its derivation is as follows:

$$\begin{aligned} P_w(d, v) &= \Pr(\hat{d} + \tau_0 \hat{v} < \lambda; d, v) \\ &= \Pr((d + \varepsilon_d) + \tau_0(v + \varepsilon_v) < \lambda; d, v) \\ &= \Pr\left(-\frac{\varepsilon_d + \tau_0 \varepsilon_v}{\sigma_Z} > \frac{d + \tau_0 v - \lambda}{\sigma_Z}; d, v\right) \\ &= Q((d + \tau_0 v - \lambda)/\sigma_Z), \end{aligned} \quad (21)$$

where σ_Z^2 is the variance of $\varepsilon_d + \tau_0 \varepsilon_v$, which is a weighted sum of range and velocity error variances, given by

$$\sigma_Z^2 = \sigma_d^2 + \tau_0^2 \sigma_v^2. \quad (22)$$

We define σ_Z^2 as range-velocity joint error index (called error index for short). The univariate Q-function $Q(x)$ is given by

$$Q(x) = \frac{1}{\sqrt{2\pi}} \int_x^\infty \exp\left(-\frac{t^2}{2}\right) dt. \quad (23)$$

Similarly, we can obtain the probability $P_w(d, v)$ for negative $d + \tau_0 v$. The complete expression of $P_w(d, v)$ is

$$P_w(d, v) = \begin{cases} Q((d + \tau_0 v - \lambda)/\sigma_Z), & d + \tau_0 v \geq 0, \\ Q(-(d + \tau_0 v - \lambda)/\sigma_Z), & d + \tau_0 v < 0. \end{cases} \quad (24)$$

The result (24) indicates that $P_w(d, v)$ depends on the decision threshold λ and square root of error index σ_Z . Therefore, when the integral domain D and manually designed PWDL $u(d, v)$ are fixed, the TWDL U shown in (20) also depends on the variables λ and σ_Z . We use the notation $U(\lambda, \sigma_Z)$ to show this dependence.

Based on the loss function $U(\lambda, \sigma_Z)$, we will tune the parameter λ and reveal how the radar performance influence the performance of CWS in the sequel.

C. Relationship between CWS and radar performance

As shown in Section III-A, the threshold λ is tunable. For a specific σ_Z , we tune it to $\tilde{\lambda}(\sigma_Z)$ to minimize TWDL, i.e.,

$$\tilde{\lambda}(\sigma_Z) = \arg \min_{\lambda} U(\lambda, \sigma_Z). \quad (25)$$

The optimal threshold $\tilde{\lambda}(\sigma_Z)$ yields an optimal decision rule in terms of TWDL. We define the corresponding minimal TWDL as MTWDL, denoted by \tilde{U} . That is,

$$\tilde{U}(\sigma_Z) = U(\tilde{\lambda}(\sigma_Z), \sigma_Z). \quad (26)$$

As with TWDL, MTWDL also balances wrong decisions within overall situations. It is obtained by tuning the decision threshold to its optimum. Therefore, we use MTWDL as the performance metric of the CWS. Note that \tilde{U} is a function of σ_Z , while σ_Z is decided by the radar performance, as shown in (22). Therefore, the function $\tilde{U}(\sigma_Z)$ establishes the desired relationship between performances of the system and radar.

Recall that the error index σ_Z^2 is the variance of $\hat{d} + \tau_0 \hat{v}$, i.e., the estimate of $d + \tau_0 v$. As shown in (15) and (19), the

two hypotheses are defined based on $d + \tau_0 v$ and the system makes decision based on its estimation. One intuition is that a more accurate estimate of $d + \tau_0 v$, in terms of smaller σ_Z^2 , leads to a system with better performance. This intuition is strictly verified by the following theorem:

Theorem 1. *The MTWDL $\tilde{U}(\sigma_Z)$ is a monotonically increasing function of σ_Z if the following conditions are satisfied:*

- 1) *In the domain D , $u(d, v) > 0$ for all (d, v) .*
- 2) *The function $u(d, v)$ is Lebesgue integrable over D .*
- 3) *The domain D is bounded.*

Proof. See Appendix C. □

In Theorem 1, we impose mild conditions on the manually designed function $u(d, v)$, so it holds for a wild range of $u(d, v)$. It is implied that a smaller σ_Z^2 yields better CWS performance in terms of MTWDL. Moreover, (13) indicates that when waveform TBP is limited, there is a tradeoff of accuracies between range and velocity. Therefore, we should design the radar waveform parameters in the aim of minimizing σ_Z^2 , such that the tradeoff that optimizes system performance is achieved. The quantitative relationship between the radar and system performance revealed in this theorem inspires the waveform design method presented in the following section.

IV. OPTIMIZED WAVEFORM PARAMETER DESIGN

According to Theorem 1, in order to achieve the best system performance, we optimize the waveform parameters W and T by minimizing the error index. For this purpose, we formulate the parameter optimization problem and analyze its results in Section IV-A; We compare the optimized parameters with conventional designs for automotive radars in Section IV-B.

A. Formulation of parameter optimization

First, we substitute (12) into (22). Hence, the error index depends on the bandwidth W and duration T as follows:

$$\sigma_Z^2 = \sigma_d^2 + \tau_0^2 \sigma_v^2 = \frac{3c^2}{8\pi^2\gamma} \left(\frac{1}{W^2} + \frac{\tau_0^2}{f_0^2} \frac{1}{T^2} \right). \quad (27)$$

Therefore, the parameter design problem can be given by

$$\begin{aligned} \min_{W, T} \quad & \sigma_Z^2 = \frac{3c^2}{8\pi^2\gamma} \left(\frac{1}{W^2} + \frac{\tau_0^2}{f_0^2} \frac{1}{T^2} \right), \\ \text{s.t.} \quad & \text{(C1)} \quad 0 < W \leq W_{\max}, 0 < T \leq T_{\max}, \\ & \text{(C2)} \quad WT \leq S. \end{aligned} \quad (28)$$

Here, we impose the following constraints on the optimization:

- (C1) The variables W and T are bounded. The upper bounds are interpreted as follows: First, the bandwidth available to all automotive radars is W_{\max} , which upper bounds W . Second, there is a requirement on the update rate of measurement, and the duration of the waveform cannot exceed the update period T_{\max} .
- (C2) The TBP of the waveform WT is no greater than a TBP limit S , in order to limit resource occupation of the radar. In practice, S is set according to the number of coexisting radars N_r , such that $N_r S \leq W_{\max} T_{\max}$.

Moreover, in Section II, possible values of T are MT_0 , where M is an integer. In the optimization problem (28),

however, we treat T as a continuous variable since T_0 is far smaller than T and the change of T over M is relatively small.

To solve (28), we first assume that W_{\max} and T_{\max} are reasonably large, such that W and T take their optima when the constraint (C1) is inactive. Using the inequality of arithmetic and geometric means, we have

$$\sigma_Z^2 \geq \frac{3c^2}{8\pi^2\gamma} \frac{2\tau_0}{f_0WT} \geq \frac{3c^2\tau_0}{4\pi^2\gamma f_0S} = \sigma_{Z,\text{opt}}^2, \quad (29)$$

where $\sigma_{Z,\text{opt}}^2$ denotes the optimal error index. The equality holds if and only if

$$W = W_{\text{opt}} = \sqrt{f_0S/\tau_0}, T = T_{\text{opt}} = \sqrt{\tau_0S/f_0}. \quad (30)$$

The solution (30) is optimal as long as $W_{\text{opt}} \leq W_{\max}$ and $T_{\text{opt}} \leq T_{\max}$. In the case that $W_{\text{opt}} > W_{\max}$ or $T_{\text{opt}} > T_{\max}$ (At most one of the two situations may happen since we require $S \leq W_{\max}T_{\max}$), the corresponding solution is

$$\begin{aligned} W &= W_{\max}, T = S/W_{\max}, & \text{if } W_{\text{opt}} > W_{\max}, \\ W &= S/T_{\max}, T = T_{\max}, & \text{if } T_{\text{opt}} > T_{\max}. \end{aligned} \quad (31)$$

In practice, $W_{\text{opt}} \leq W_{\max}, T_{\text{opt}} \leq T_{\max}$ is the general case and will be analyzed in the remainder.

The following two observations are made about the optimization results in (29) and (30): First, when the other parameters are fixed, the optimal error index $\sigma_{Z,\text{opt}}^2$ is inversely proportional to the SNR γ and TBP S . Second, the ratio of optimal bandwidth and duration is $W_{\text{opt}}/T_{\text{opt}} = f_0/\tau_0$, which is invariant of γ and S . This ratio reflects the tradeoff between bandwidth and duration when the TBP is limited.

B. Comparison between optimized and conventional design

In this section, we compare the waveform optimization strategy in Section IV with some existing approaches in the terms of CWS performance and resource efficiency.

We consider some state-of-the-art waveform designs for automotive radars [20]–[23]. The routine of parameter design is as follows: First, requirements on range resolution Δ_d and velocity resolution Δ_v are proposed empirically. Then, the designed bandwidth W_{con} and duration T_{con} are given by

$$W_{\text{con}} = c/(2\Delta_d), T_{\text{con}} = c/(2f_0\Delta_v). \quad (32)$$

The corresponding waveform TBP is $S_{\text{con}} = c^2/(4f_0\Delta_d\Delta_v)$. To facilitate the comparison with our method, we calculate the error index introduced for the conventional approach, given by

$$\sigma_{Z,\text{con}}^2 = \frac{3c^2\tau_0}{8\pi^2\gamma f_0S_{\text{con}}} \left(\frac{\Delta_d}{\tau_0\Delta_v} + \frac{\tau_0\Delta_v}{\Delta_d} \right). \quad (33)$$

In these methods, the bandwidth and duration of the waveform are designed separately. The issue of limited electromagnetic resources and the tradeoff of estimation accuracy between range and velocity are barely considered.

We now compare between the proposed and the conventional waveform design methods. In particular, we consider the parameters of error index, TBP and SNR, representing the CWS performance, electromagnetic resource efficiency and energy efficiency, respectively. We analyze the influence on one parameter of the design approaches when the rest parameters are fixed. Details of comparisons are as follows:

1) Comparison on error index with SNR and TBP fixed

When the SNR γ is fixed and TBP is set as S_{con} , the results of optimized design are obtained using (30) and (29). Further, we compare the error indices of two designs as follows:

$$\frac{\sigma_{Z,\text{opt}}^2}{\sigma_{Z,\text{con}}^2} = \frac{2\tau_0 \cdot \Delta_d/\Delta_v}{\tau_0^2 + (\Delta_d/\Delta_v)^2}. \quad (34)$$

A deduction from (34) is that $\sigma_{Z,\text{opt}}^2 < \sigma_{Z,\text{con}}^2$ as long as $\tau_0 \neq \Delta_d/\Delta_v$. That is, the optimized design reduces the error index and further improves the CWS performance. To be specific, τ_0 is the TTC threshold of CWS, whose typical values are 3 to 5 seconds (see [41] and the references therein). The expression Δ_d/Δ_v is the ratio of conventional range and velocity resolution, whose typical values are 0.7 to 1.2 seconds [20]–[23]. Thus, τ_0 is greater than Δ_d/Δ_v in practice.

2) Comparison on TBP with SNR and error index fixed

In conventional design, after Δ_d and Δ_v are specified, the bandwidth and duration are designed. Then, $\sigma_{Z,\text{opt}}^2$ is given by (33), which decides the CWS performance. Here, we study how much TBP is required using the optimized design to achieve the same performance as conventional design. Using (29), we obtain the TBP S_{opt} to yield an error index equal to $\sigma_{Z,\text{opt}}^2$. The ratio of two TBPs is

$$\frac{S_{\text{opt}}}{S_{\text{con}}} = \frac{2\tau_0 \cdot \Delta_d/\Delta_v}{\tau_0^2 + (\Delta_d/\Delta_v)^2}. \quad (35)$$

The result of this ratio is the same as (34) and we have $S_{\text{opt}} < S_{\text{con}}$ as long as $\tau_0 \neq \Delta_d/\Delta_v$. It means that the optimized design can reduce waveform TBP while the system performance remains the same.

3) Comparison on SNR with TBP and error index fixed

We study what level of SNR is required using the optimized design to achieve the same performance as conventional design. For a specific error index σ_Z^2 and TBP S , we obtain the required SNR for optimized and conventional design using (29) and (33), denoted by γ_{opt} and γ_{con} . Their ratio is

$$\frac{\gamma_{\text{opt}}}{\gamma_{\text{con}}} = \frac{2\tau_0 \cdot \Delta_d/\Delta_v}{\tau_0^2 + (\Delta_d/\Delta_v)^2}. \quad (36)$$

Again, the ratio is the same as (34), and $\gamma_{\text{opt}} < \gamma_{\text{con}}$ as long as $\tau_0 \neq \Delta_d/\Delta_v$. That is, the optimized design can achieve the same system performance as conventional design with lower transmitted power.

To summarize, the above comparisons illustrate the advantages of optimized parameter design from three aspects, namely, performance improvement, resource efficiency and energy efficiency. These advantages are further demonstrated through simulations in the Section V.

V. NUMERICAL RESULTS

In this section, we use numerical results to verify previous assumptions and to compare the optimized and conventional parameter design. This section is divided into the following five parts: First, we introduce settings of the simulation in Section V-A. Second, we compare the GLRT rule and approximate rule in Section V-B. Third, we compare the error indices of the two designs in Section V-C. Fourth, we study the

performance metric MTWDL as a function of TBP in Section V-D to compare the resource efficiency of the two designs. Finally, the MTWDL is demonstrated as a function of SNR in Section V-E to compare the energy efficiency.

A. Simulation settings

The system and waveform parameters are specified as follows: $f_0 = 24$ GHz and $\tau_0 = 4$ s (as suggested in [41]). The maximum bandwidth and duration, i.e., W_{\max} and T_{\max} , are set as 500 MHz and 50 ms. For conventional design, the range and velocity resolution are $\Delta_d = 0.5$ m and $\Delta_v = 0.6$ m/s, as suggested in [21]. The corresponding waveform parameters are $W_{\text{con}} = 300$ MHz and $T_{\text{con}} = 10.4$ ms, and the TBP is $S_{\text{con}} = 3.125 \times 10^6$. For optimized design, the waveform bandwidth and duration are designed by solving (28) given the TBP. Specifically, when the TBP is S_{con} , the optimized parameters are $W_{\text{opt}} = 137$ MHz and $T_{\text{opt}} = 22.8$ ms.

As for the TWDL, the domain of interest D is $D : 0.1 \text{ m} \leq d \leq 100 \text{ m}, -30 \text{ m/s} \leq v \leq 30 \text{ m/s}$. We consider the PWDL in the following forms:

- 1) Constant loss: The loss of false alarm and miss are two different constants, i.e.,

$$u(d, v) = \begin{cases} 1, & d + \tau_0 v \geq 0, \\ u_1, & d + \tau_0 v < 0, \end{cases} \quad (37)$$

where u_1 reflects the severity of miss relative to false alarm. Specifically, we set u_1 as 5 and 10, corresponding to PWDL 1 and PWDL 2, respectively.

- 2) TTC-dependent loss: Since the TTC reflects the urgency of warning [45], the loss function $u(d, v)$ can be designed based on the TTC. One example is

$$u(d, v) = \begin{cases} 1, & d + \tau_0 v \geq 0, \\ u_2 \cdot (-v/d), & d + \tau_0 v < 0. \end{cases} \quad (38)$$

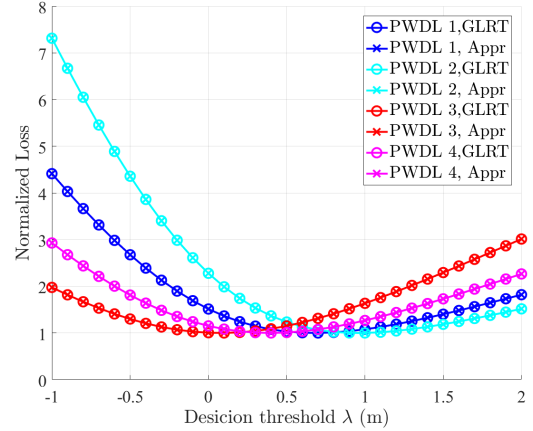
We set u_2 as 5 s and 10 s, corresponding to PWDL 3 and PWDL 4, respectively.

B. Comparison between the GLRT and approximate rule

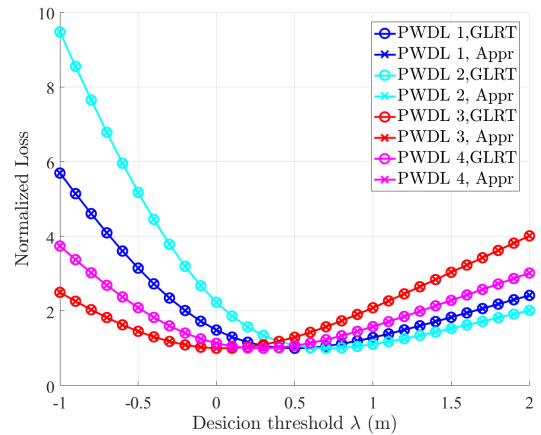
In Section III, we state that the performance of the GLRT and approximate rule is close and conduct theoretical analysis based on the approximate rule. Here, we use simulations to verify this statement.

When we fix the TBP S as S_{con} and SNR γ as 20 dB, we can obtain the parameters of conventional and optimized design, as shown in Section V-A, and the variances, σ_d^2 and σ_v^2 , according to (13). Further, the probability $P_w(d, v)$ can be obtained through numerical integration for the GLRT rule, while $P_w(d, v)$ is given by (24) for the approximate rule. Finally, the TWDL U can be obtained through the integration in (20) with different decision thresholds λ .

For two configurations of waveform parameters and four PWDL functions, we obtain the TWDL using both the GLRT and approximate rule as a function of the threshold λ and the results are shown in Fig. 3. Two types of markers are used to distinguish the GLRT rule (circle marker) and approximate rule (cross marker, abbreviated as Appr in the legends). Additionally, for each PWDL, the TWDL is divided by the minimal



(a) Conventional design: $W_{\text{con}} = 300$ MHz, $T_{\text{con}} = 10.4$ ms.



(b) Optimized design: $W_{\text{opt}} = 137$ MHz, $T_{\text{opt}} = 22.8$ ms.

Fig. 3. Comparison of TWDL using GLRT and approximate rule with two waveform configurations and four PWDL functions (SNR $\gamma = 20$ dB).

TWDL over all λ using the GLRT rule for normalization. The results show that the normalized losses of these two rules are almost identical, thereby verifying our statement.

C. Comparison on error index

When we fix the TBP as $S_{\text{con}} = 3.125 \times 10^6$ and SNR as $\gamma = 20$ dB, there are different designs of bandwidth W and duration T that satisfy $WT = S_{\text{con}}$. For each design, the theoretical result of error index σ_Z^2 can be obtained using (27), and σ_Z^2 is demonstrated as a function of W in Fig. 4. Moreover, the conventional and optimized design are given in V-A and marked as a triangle and a circle, respectively. It is shown that the error index of optimized design is 4.0 dB lower than conventional design, and this difference is decided by the TTC threshold τ_0 and conventional resolution ratio Δ_d/Δ_v , as indicated in (34). The smaller σ_Z^2 leads to a better CWS performance, which is illustrated in the following simulations.

D. Comparison on MTWDL versus TBP

Fig. 5 illustrates the CWS performance metric as a function of TBP and helps compare resource efficiencies of the two designs. Details of this figure are explained in the following.

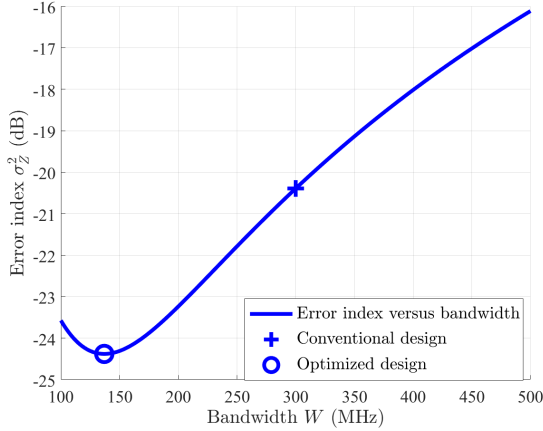


Fig. 4. Error index σ_z^2 versus bandwidth W with fixed TBP.

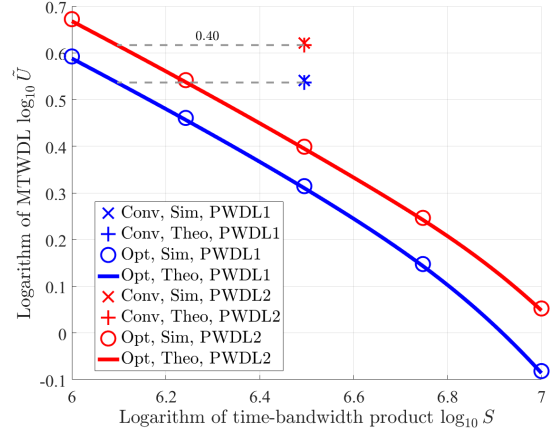
As for the conventional design (abbreviated as Conv in the legends), the bandwidth and duration are described in Section V-A. Further, MTWDL \tilde{U} is obtained in two ways. First, we obtain the simulated results (abbreviated as Sim). We use the signal model (6) to generate noisy observations and obtain samples of estimates through MLE. These samples are used to get the probability $P_w(d, v)$ for different thresholds λ and then the TWDL U . The smallest U over λ is chosen as the MTWDL \tilde{U} . These simulated results are marked as plus signs in Fig. 5. Second, we obtain the theoretical results (abbreviated as Theo). The probability $P_w(d, v)$ is obtained by substituting σ_z^2 into (24), and U with specific λ is obtained through integration described in (20). Again, \tilde{U} is the smallest U . These theoretical results are marked as crosses in Fig. 5.

As for the optimized design (abbreviated as Opt), with TBP varying from 1×10^6 to 1×10^7 , the corresponding optimized bandwidth and duration are solution of (28). Similarly, we obtain both simulated and theoretical results of \tilde{U} , which are marked as circles and plotted as curves in Fig. 5, respectively.

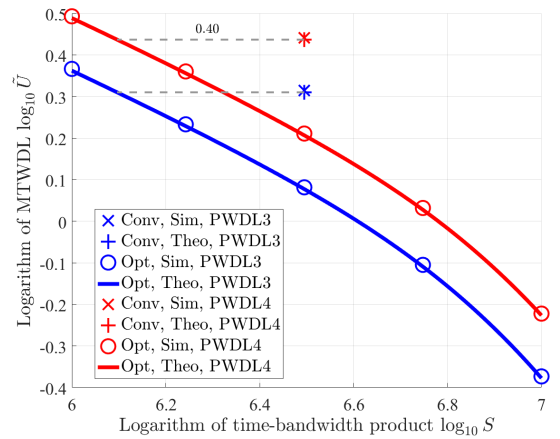
Our first observation is that our theoretical results fit the simulated results well under this SNR. Moreover, when the TBP is fixed, the optimized design yields a better performance of the CWS in terms of MTWDL. On the other hand, to achieve a certain performance of CWS, the logarithm of required TBP $\log_{10} S$ using the optimized parameter design is 0.40 less than that using the conventional design. Equivalently, the required TBP of optimized design is 0.40 times that of conventional design while the CWS performance remains unchanged, which conforms to the result (35). This observation indicates the remarkable advantage of the optimized design in resource efficiency. To be specific, in the non-overlapped allocation scheme, the number of radars that can simultaneously operate in the same place with no mutual interference can be increased by 150% using the optimized design while the CWS performance remains the same as the conventional design.

E. Comparison on MTWDL versus SNR

To demonstrate that the optimized design can reduce radar power, we show MTWDL \tilde{U} as a function of SNR in Fig. 6. The fixed TBP is S_{con} . The corresponding conventional and optimized design are given in Section V-A. As the SNR γ



(a) PWDL 1 and PWDL 2.



(b) PWDL 3 and PWDL 4.

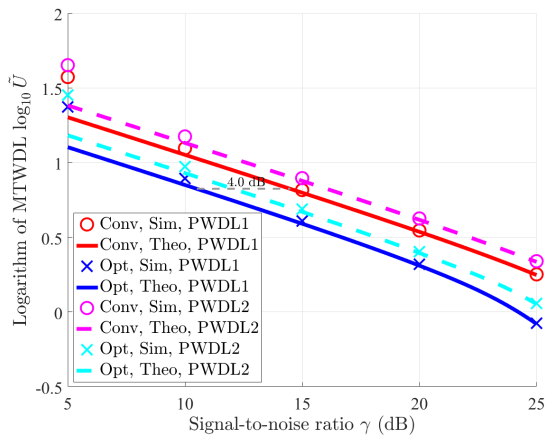
Fig. 5. Performance metric \tilde{U} as a function of TBP S .

varies from 5 dB to 25 dB, the MTWDL \tilde{U} are obtained. Similarly to Section V-D, both simulated and theoretical results are shown.

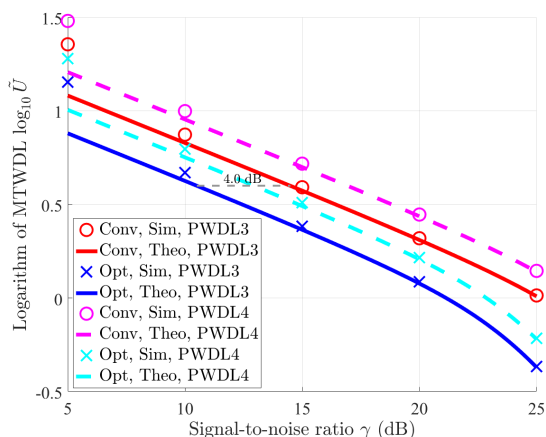
First, Fig. 6 shows that the theoretical analysis fits the simulated results well when the SNR is greater than 10 dB. Such an SNR level is a common case in practice [21]. Moreover, the optimized design outperforms the conventional design in terms of MTWDL \tilde{U} . On the other hand, with TBP fixed, the transmit power of the radar can be reduced by 4.0 dB to reach a certain system performance using the optimized parameters. This result can be also deduced from (36).

VI. CONCLUSION AND OUTLOOK

Facing the increasing tension of electromagnetic resources on the road, we propose a method of radar parameter design oriented to the performance of CWS, which enables the radar to use the limited resources more efficiently. For this purpose, we propose the MTWDL as the performance metric of CWS and establish its relationship with the performance of radar. Our analysis shows that in order to achieve the optimal performance of the CWS, we design the waveform bandwidth and duration to reduce the defined error index. Accordingly, we formulate the optimization on bandwidth and duration



(a) PWDL 1 and PWDL 2.



(b) PWDL 3 and PWDL 4.

Fig. 6. Performance metric \tilde{U} as a function of SNR γ .

to minimize the error index with limited resources, which is quantified by TBP. Both theoretical and numerical results show that the proposed method improves resource or energy efficiency compared with conventional parameter designs.

Establishment of the relationship between the performance of intelligent automotive systems and automotive radar waveform parameters is an important issue. It provides a deeper understanding of how many resources are needed and how to make full use of them. Future studies may involve more kinds of automotive systems, e.g., ACC systems, and give a further insight into the waveform design of automotive radar.

APPENDIX A

CRLB FOR ESTIMATING RANGE AND VELOCITY

In order to obtain the CRLB for estimating θ_k from observations (8), we first derive the CRLB for ξ , because θ_k is a linear transform of ξ . The CRLB for θ_k is then obtained based on the results of ξ . Making some approximations on this CRLB under the assumption that M is sufficiently large, yields the result in Proposition 1.

When we calculate the CRLB for ξ , our analysis is as follows: First, we calculate the Fisher information matrix (FIM) for ξ , which is the inverse of the CRLB. Second, we

prove that the FIM can be approximated as a block diagonal matrix with large N and M , which facilitates the subsequent inverse operation on the FIM and implies the CRLB for ξ .

Estimating ξ from $N \times M$ observations, as shown in (8), is a problem of estimating two-dimensional frequencies [38]. As defined in Section II-A, the parameter to be estimated ξ is written as $\xi = [\xi_1^T, \xi_2^T, \dots, \xi_K^T]^T$, where $\xi_k = [b_k, \psi_k, f_{1,k}, f_{2,k}]^T$. Here, variables b_k and ψ_k denote the amplitude and initial phase of the k -th two-dimensional frequency component, while $f_{1,k}$ and $f_{2,k}$ are its two-dimensional frequencies. The FIM for ξ , denoted as \mathbf{F} , is a $4K \times 4K$ matrix, which can be divided into $K^2 4 \times 4$ submatrices, i.e.,

$$\mathbf{F} = \begin{bmatrix} \mathbf{F}_{11} & \cdots & \mathbf{F}_{1K} \\ \vdots & \ddots & \vdots \\ \mathbf{F}_{K1} & \cdots & \mathbf{F}_{KK} \end{bmatrix}. \quad (39)$$

According to [38], the submatrix $\mathbf{F}_{k_1 k_2}$ is given by (40). Here, $X_{k_1 k_2}^{(l_0, l_1, l_2)}(k_1 = 1, 2, \dots, K, k_2 = 1, 2, \dots, K)$ is given by

$$X_{k_1 k_2}^{(l_0, l_1, l_2)} = \sum_{n=0}^{N-1} \sum_{m=0}^{M-1} (2\pi n)^{l_1} (2\pi m)^{l_2} g_{l_0}(\Delta\psi + 2\pi\Delta f_1 n + 2\pi\Delta f_2 m), \quad (41)$$

where we define $g_{l_0}(x) = \cos(x)$ when $l_0 = 0$ and $g_{l_0}(x) = \sin(x)$ when $l_0 = 1$. The three new variables are defined as $\Delta\psi = \psi_{k_1} - \psi_{k_2}$, $\Delta f_1 = f_{1,k_1} - f_{1,k_2}$ and $\Delta f_2 = f_{2,k_1} - f_{2,k_2}$. Here, we drop the their dependence of on k_1 and k_2 for simplicity of notation.

To study the asymptotic property of \mathbf{F} , we simplify the expression of $X_{k_1 k_2}^{(l_0, l_1, l_2)}$. First, when $l_1 = l_2 = 0$, we have

$$X_{k_1 k_2}^{(l_0, 0, 0)} = \frac{\sin(\pi N \Delta f_1)}{\sin(\pi \Delta f_1)} \frac{\sin(\pi M \Delta f_2)}{\sin(\pi \Delta f_2)} \cdot g_{l_0}(\Delta\psi + 2\pi(N-1)\Delta f_1 + 2\pi(M-1)\Delta f_2). \quad (42)$$

When $l_1 \neq 0$ or $l_2 \neq 0$, $X_{k_1 k_2}^{(l_0, l_1, l_2)}$ is the partial differential of $X_{k_1 k_2}^{(l_0, 0, 0)}$ or $X_{k_1 k_2}^{(1, 0, 0)}$ over Δf_1 and Δf_2 , given by

$$X_{k_1 k_2}^{(l_0, l_1, l_2)} = (-1)^{l_3} \frac{\partial^{l_1+l_2} X_{k_1 k_2}^{(l_0, 0, 0)}}{(\partial \Delta f_1)^{l_1} (\partial \Delta f_2)^{l_2}}, \quad (43)$$

where $l_0^{(0)} = l_0 + l_1 + l_2 \pmod{2}$ ($p \pmod{q}$ denotes the remainder after division of p by q) and $l_3 = \lfloor (l_1 + l_2 + 1 - l_0^{(0)})/2 \rfloor$ ($\lfloor x \rfloor$ denotes the nearest integer less than or equal to x).

To summarize the existing results, (39), (40), (42) and (43) jointly give the FIM for ξ , i.e., \mathbf{F} . Specifically, (39) partitions \mathbf{F} into submatrices; (40) shows the entries of each submatrix; (42) and (43) give the simplified results of these entries.

The CRLB is the inverse of \mathbf{F} [35]. However, it is difficult to obtain an analytical expression for the inverse. In the following, we show that \mathbf{F} can be approximated as a block diagonal matrix when N and M approach infinity, which enables us to solve the inverse analytically.

We analyze the entries of $\mathbf{F}_{k_1 k_2}$ shown in (40) when N and M tend to infinity. As a result, we have

$$\lim_{\substack{N \rightarrow \infty \\ M \rightarrow \infty}} \frac{X_{k_1 k_2}^{(l_0, l_1, l_2)}}{N^{l_1+1} M^{l_2+1}} = \frac{(2\pi)^{l_1+l_2}}{(l_1+1)(l_2+1)} \delta_{l_0} \delta_{k_1-k_2}, \quad (44)$$

where δ_k is the discrete delta function, i.e., $\delta_k = 1$ when $k = 0$ and $\delta_k = 0$ for the other values of k . That is, the

$$\mathbf{F}_{k_1 k_2} = \frac{2}{\sigma_w^2} \begin{bmatrix} X_{k_1 k_2}^{(0,0,0)} & b_{k_2} X_{k_1 k_2}^{(1,0,0)} & b_{k_2} X_{k_1 k_2}^{(1,1,0)} & b_{k_2} X_{k_1 k_2}^{(1,0,1)} \\ -b_{k_1} X_{k_1 k_2}^{(1,0,0)} & b_{k_1} b_{k_2} X_{k_1 k_2}^{(0,0,0)} & b_{k_1} b_{k_2} X_{k_1 k_2}^{(0,1,0)} & b_{k_1} b_{k_2} X_{k_1 k_2}^{(0,0,1)} \\ -b_{k_1} X_{k_1 k_2}^{(1,1,0)} & b_{k_1} b_{k_2} X_{k_1 k_2}^{(0,1,0)} & b_{k_1} b_{k_2} X_{k_1 k_2}^{(0,2,0)} & b_{k_1} b_{k_2} X_{k_1 k_2}^{(0,1,1)} \\ -b_{k_1} X_{k_1 k_2}^{(1,0,1)} & b_{k_1} b_{k_2} X_{k_1 k_2}^{(0,0,1)} & b_{k_1} b_{k_2} X_{k_1 k_2}^{(0,1,1)} & b_{k_1} b_{k_2} X_{k_1 k_2}^{(0,0,2)} \end{bmatrix}. \quad (40)$$

limits are non-zero only if k_1 equals k_2 , implying that the non-diagonal submatrices of \mathbf{F} are negligible relative to the diagonal submatrices. Further, we introduce the matrix:

$$\mathbf{\Lambda}_k = \text{diag} \left(\sqrt{NM}, b_k \sqrt{NM}, b_k \sqrt{N^3 M}, b_k \sqrt{NM^3} \right). \quad (45)$$

Based on the limits shown in (44), we can get

$$\lim_{\substack{N \rightarrow \infty \\ M \rightarrow \infty}} \mathbf{\Lambda}_{k_1}^{-1} \mathbf{F}_{k_1 k_2} \mathbf{\Lambda}_{k_2}^{-1} = 2\sigma_w^{-2} \delta_{k_1 - k_2} \mathbf{C}, \quad (46)$$

where the constant matrix \mathbf{C} is

$$\mathbf{C} = \begin{bmatrix} 1 & 0 & 0 & 0 \\ 0 & 1 & \pi & \pi \\ 0 & \pi & 4\pi^2/3 & \pi^2 \\ 0 & \pi & \pi^2 & 4\pi^2/3 \end{bmatrix}, \quad (47)$$

According to (46), when N and M are sufficiently large, we can approximate the submatrix $\mathbf{F}_{k_1 k_2}$ as $\mathbf{F}_{k_1 k_2}^{(\infty)}$, given by

$$\mathbf{F}_{k_1 k_2}^{(\infty)} = 2\sigma_w^{-2} \delta_{k_1 - k_2} \mathbf{\Lambda}_{k_1} \mathbf{C} \mathbf{\Lambda}_{k_2}. \quad (48)$$

The delta function in (48) indicates that the FIM \mathbf{F} can be approximated as a diagonal matrix as follows:

$$\begin{aligned} \mathbf{F}^{(\infty)} &= \text{diag} \left(\mathbf{F}_{11}^{(\infty)}, \mathbf{F}_{22}^{(\infty)}, \dots, \mathbf{F}_{KK}^{(\infty)} \right) \\ &= 2\sigma_w^{-2} \text{diag} (\mathbf{\Lambda}_1 \mathbf{C} \mathbf{\Lambda}_1, \mathbf{\Lambda}_2 \mathbf{C} \mathbf{\Lambda}_2, \dots, \mathbf{\Lambda}_K \mathbf{C} \mathbf{\Lambda}_K). \end{aligned} \quad (49)$$

Combining (45) and (47), the submatrix $\mathbf{\Lambda}_k \mathbf{C} \mathbf{\Lambda}_k$ is given by

$$\mathbf{\Lambda}_k \mathbf{C} \mathbf{\Lambda}_k = \begin{bmatrix} NM & 0 & 0 & 0 \\ 0 & b_k^2 NM & \pi b_k^2 N^2 M & \pi b_k^2 NM^2 \\ 0 & \pi b_k^2 N^2 M & \frac{4\pi^2}{3} b_k^2 N^3 M & \pi^2 b_k^2 N^2 M^2 \\ 0 & \pi b_k^2 NM^2 & \pi^2 b_k^2 N^2 M^2 & \frac{4\pi^2}{3} b_k^2 NM^3 \end{bmatrix}.$$

We have approximated the FIM as a block diagonal matrix $\mathbf{F}^{(\infty)}$, as shown in (49). The asymptotic CRLB for $\boldsymbol{\xi}$ is the inverse of $\mathbf{F}^{(\infty)}$ and it is also a diagonal matrix, given by

$$\mathbf{B}_\xi = \text{diag} (\mathbf{B}_{\xi,1}, \mathbf{B}_{\xi,2}, \dots, \mathbf{B}_{\xi,K}), \quad (50)$$

where $\mathbf{B}_{\xi,k}$ is the inverse of the counterpart in (49), given by

$$\begin{aligned} \mathbf{B}_{\xi,k} &= (2\sigma_w^{-2} \mathbf{\Lambda}_k \mathbf{C} \mathbf{\Lambda}_k)^{-1} \\ &= \frac{\sigma_w^2}{2A^2 |\alpha_k|^2 NM} \begin{bmatrix} A^2 |\alpha_k|^2 & 0 & 0 & 0 \\ 0 & 7 & -\frac{3}{\pi N} & -\frac{3}{\pi M} \\ 0 & -\frac{3}{\pi N} & \frac{3}{\pi^2 N^2} & 0 \\ 0 & -\frac{3}{\pi M} & 0 & \frac{3}{\pi^2 M^2} \end{bmatrix}. \end{aligned}$$

The block diagonal structure of the CRLB \mathbf{B}_ξ means that the estimation errors of $\boldsymbol{\xi}_k$ with different k are asymptotically uncorrelated when N and M are sufficiently large. In other words, the CRLB for parameter estimation of one scatterer can be considered not influenced by others.

As mentioned in Section II-A, the estimate of range and velocity of the k -th scatterer, formulated as $\boldsymbol{\theta}_k = [\hat{d}_k, \hat{v}_k]^T$, is

obtained using the estimate of two-dimensional frequencies, formulated as $\hat{\mathbf{f}}_k = [\hat{f}_{1,k}, \hat{f}_{2,k}]^T$. To be specific, according to (5) and (7), $\hat{\boldsymbol{\theta}}_k$ is a linear combination of $\hat{\mathbf{f}}_k$, given by,

$$\hat{\boldsymbol{\theta}}_k = \frac{c}{2} \begin{bmatrix} N/W & -1/W \\ 0 & 1/(f_0 T_0) \end{bmatrix} \hat{\mathbf{f}}_k \quad (51)$$

Thus, the CRLB for $\boldsymbol{\theta}_k$ is obtained based on the CRLB for $\mathbf{f}_k = [f_{1,k}, f_{2,k}]^T$, which is contained in \mathbf{B}_ξ . As a result, its asymptotic CRLB is

$$\mathbf{B}_{\boldsymbol{\theta},k}^{(0)} = \frac{3c^2}{8\pi^2 \gamma_k} \begin{bmatrix} \left(1 + \frac{1}{M^2}\right) \frac{1}{W^2} & -\frac{1}{f_0 T_0 W M^2} \\ -\frac{1}{f_0 T_0 W M^2} & \frac{1}{f_0^2 T^2} \end{bmatrix}. \quad (52)$$

To simplify the expression of CRLB in (52), we conduct some approximations on $\mathbf{B}_{\boldsymbol{\theta},k}^{(0)}$ for large M . First, the CRLB of d_k is $\frac{3c^2}{8\pi^2 \gamma_k} \left(1 + \frac{1}{M^2}\right) \frac{1}{W^2}$, which can be approximated as $\frac{3c^2}{8\pi^2 \gamma_k} \frac{1}{W^2}$ with large M . Second, the correlation coefficient of estimation errors of d_k and v_k is $\frac{1}{\sqrt{M^2+1}}$ and it approaches 0 when M is sufficiently large, which means that estimation errors of d_k and v_k are asymptotically uncorrelated. Therefore, the CRLB for $\boldsymbol{\theta}_k$ can be approximated as the diagonal matrix shown in (11). The result in (11) can also be obtained using the stop-and-hop assumption, which is reasonable in automotive applications since the velocities of the vehicle and scatterers are much lower than the speed of light [18].

APPENDIX B DERIVATIONS OF THE GLRT RULE

The first step of GLRT is to calculate the likelihood ratio \mathcal{L}_G in GLRT based on the measurement $\hat{\boldsymbol{\theta}}$, defined as [44]

$$\mathcal{L}_G(\hat{\boldsymbol{\theta}}) = \max_{\boldsymbol{\theta}_1} p(\hat{\boldsymbol{\theta}}; \boldsymbol{\theta}_1, \mathcal{H}_1) / \max_{\boldsymbol{\theta}_0} p(\hat{\boldsymbol{\theta}}; \boldsymbol{\theta}_0, \mathcal{H}_0), \quad (53)$$

where $p(\hat{\boldsymbol{\theta}}; \boldsymbol{\theta}_i, \mathcal{H}_i)$ denotes the likelihood of $\hat{\boldsymbol{\theta}}$ given the true value $\boldsymbol{\theta}_i$ and hypothesis \mathcal{H}_i .

The second step is to make decisions by comparing the logarithm likelihood ratio (LLR) with a threshold λ_G , i.e.,

$$\ln \mathcal{L}_G(\hat{\boldsymbol{\theta}}) \underset{\mathcal{H}_0}{\overset{\mathcal{H}_1}{\gtrless}} \lambda_G. \quad (54)$$

As analyzed in Section II, the measurement error $\boldsymbol{\varepsilon}$ is assumed to be zero-mean Gaussian with covariance $\boldsymbol{\Sigma}_\varepsilon = \text{diag}(\sigma_d^2, \sigma_v^2)$. Thus, the likelihood $p(\hat{\boldsymbol{\theta}}; \boldsymbol{\theta}_i, \mathcal{H}_i)$ is given by

$$p(\hat{\boldsymbol{\theta}}; \boldsymbol{\theta}_i, \mathcal{H}_i) = \frac{1}{2\pi \sqrt{\det \boldsymbol{\Sigma}_\varepsilon}} e^{-\frac{1}{2}(\hat{\boldsymbol{\theta}} - \boldsymbol{\theta}_i)^T \boldsymbol{\Sigma}_\varepsilon^{-1} (\hat{\boldsymbol{\theta}} - \boldsymbol{\theta}_i)}.$$

The LLR is given by

$$\begin{aligned} \ln \mathcal{L}_G(\hat{\theta}) = & -\frac{1}{2} \left(\min_{\theta_1 \in \mathcal{R}_1} \left[(\hat{\theta} - \theta_1)^T \Sigma_\epsilon^{-1} (\hat{\theta} - \theta_1) \right] \right. \\ & \left. - \min_{\theta_0 \in \mathcal{R}_0} \left[(\hat{\theta} - \theta_0)^T \Sigma_\epsilon^{-1} (\hat{\theta} - \theta_0) \right] \right). \end{aligned} \quad (55)$$

Here, \mathcal{R}_i denotes the set of θ under the hypothesis \mathcal{H}_i , i.e., $\mathcal{R}_1 = \{[d, v]^T \mid d + \tau_0 v < 0, d > 0\}$ and $\mathcal{R}_0 = \{[d, v]^T \mid d + \tau_0 v \geq 0, d > 0\}$. The right side of (55) involves two minimization problems, whose solutions are given by

$$s_0(\hat{\theta}) = \min_{\theta_0 \in \mathcal{R}_0} \left[(\hat{\theta} - \theta_0)^T \Sigma_\epsilon^{-1} (\hat{\theta} - \theta_0) \right] = \begin{cases} -\frac{\hat{d} + \tau_0 \hat{v}}{\sqrt{\sigma_d^2 + \tau_0^2 \sigma_v^2}}, & \hat{d} > 0, \hat{d} < -\tau_0 \hat{v}, \\ 0, & \hat{d} > 0, \hat{d} \geq -\tau_0 \hat{v}. \end{cases}$$

$$s_1(\hat{\theta}) = \min_{\theta_1 \in \mathcal{R}_1} \left[(\hat{\theta} - \theta_1)^T \Sigma_\epsilon^{-1} (\hat{\theta} - \theta_1) \right] = \begin{cases} 0, & \hat{d} > 0, \hat{d} < -\tau_0 \hat{v} \\ \frac{\hat{d} + \tau_0 \hat{v}}{\sqrt{\sigma_d^2 + \tau_0^2 \sigma_v^2}}, & \hat{d} \geq -\tau_0 \hat{v}, \hat{d} \geq \frac{\sigma_d^2}{\sigma_v^2 \tau_0} \hat{v}, \\ \sqrt{\sigma_d^{-2} \hat{d}^2 + \sigma_v^{-2} \hat{v}^2}, & \hat{d} > 0, \hat{d} < \frac{\sigma_d^2}{\sigma_v^2 \tau_0} \hat{v}. \end{cases}$$

Combining the results above, we get the expression of the LLR for (55). Then, we multiply both sides of (54) by $-2\sqrt{\sigma_d^2 + \tau_0^2 \sigma_v^2}$, yielding $T_G(\hat{\theta}) = -2\sqrt{\sigma_d^2 + \tau_0^2 \sigma_v^2} \ln \mathcal{L}_G(\hat{\theta})$ and $\lambda = -2\sqrt{\sigma_d^2 + \tau_0^2 \sigma_v^2} \lambda_G$. Thus, the GLRT rule (54) can be transformed into (16).

APPENDIX C

MONOTONICITY OF MTWDL IN TERMS OF ERROR INDEX

We prove that $\tilde{U}(\sigma_Z)$ is a monotonically increasing function of σ_Z under the conditions stated in Theorem 1. The proof is divided into two steps: We first prove that with a fixed σ_Z , $\tilde{\lambda}(\sigma_Z)$ is the only one extremum of $U(\lambda, \sigma_Z)$. Then, we prove that the derivative $d\tilde{U}/d\sigma_Z$ is positive, indicating the increasing monotonicity of $\tilde{U}(\sigma_Z)$.

We first divide the TWDL shown in (20) into two parts:

$$U = \iint_{D_0} P_w(d, v) u(d, v) d d d v + \iint_{D_1} P_w(d, v) u(d, v) d d d v,$$

where the subdomains D_0 and D_1 are $D_0 : (d, v) \in D, d + \tau_0 v \geq 0$ and $D_1 : (d, v) \in D, d + \tau_0 v < 0$. According to (24) and the definition of Q-function (23), we conclude that $P_w(d, v)$ is a smooth function with respect to λ and σ_Z for all (d, v) . Combined with the conditions that $u(d, v)$ is Lebesgue integrable over D and D is bounded, the TWDL $U(\lambda, \sigma_Z)$ is also a smooth function of λ and σ_Z .

As mentioned in Section III-B, for a fixed σ_Z , we aim to tune the threshold λ to $\tilde{\lambda}(\sigma_Z)$ such that U reaches its minimum. To this end, we treat $U(\lambda, \sigma_Z)$ as a function of λ and conduct partial differentiation $U(\lambda, \sigma_Z)$ over λ and get the first-order and second-order derivative. The results are shown in (56) and (57). Here, we define $Z = d + \tau_0 v$.

We aim to find the minimum of $U(\lambda, \sigma_Z)$ with fixed σ_Z and an extremum is a candidate for minimum. Thus, we analyze the extrema of $U(\lambda, \sigma_Z)$ and consider any $\lambda_0(\sigma_Z)$ such that

$$\left. \frac{\partial U}{\partial \lambda} \right|_{\lambda=\lambda_0, \sigma_Z} = 0. \quad (58)$$

Combining (57), (58) and $u(d, v) > 0$, we have

$$\left. \frac{\partial^2 U}{\partial \lambda^2} \right|_{\lambda=\lambda_0, \sigma_Z} > 0. \quad (59)$$

This means that all extrema are local minima. With this result and the fact that $U(\lambda, \sigma_Z)$ is smooth, we can further conclude that $U(\lambda, \sigma_Z)$ has only one extremum, which is also the global minimum. Therefore, the optimal threshold $\tilde{\lambda}(\sigma_Z)$ satisfies

$$\left. \frac{\partial U}{\partial \lambda} \right|_{\lambda=\tilde{\lambda}(\sigma_Z), \sigma_Z} = 0. \quad (60)$$

Now we have proven that the optimal threshold $\tilde{\lambda}(\sigma_Z)$ is the only one extremum of $U(\lambda, \sigma_Z)$ for a fixed σ_Z . After $\tilde{\lambda}(\sigma_Z)$ is obtained, the minimal U is a function of σ_Z , i.e., $\tilde{U}(\sigma_Z) = U(\tilde{\lambda}(\sigma_Z), \sigma_Z)$. Our main concern is the monotonicity of $\tilde{U}(\sigma_Z)$. With the chain rule, its derivative is as follows:

$$\frac{d\tilde{U}}{d\sigma_Z} = \left. \frac{\partial U}{\partial \lambda} \right|_{\lambda=\tilde{\lambda}} \cdot \frac{\partial \tilde{\lambda}}{\partial \sigma_Z} + \left. \frac{\partial U}{\partial \sigma_Z} \right|_{\lambda=\tilde{\lambda}} = \left. \frac{\partial U}{\partial \sigma_Z} \right|_{\lambda=\tilde{\lambda}}. \quad (61)$$

Note that the above deduction uses the result (60). The partial differential $\partial U / \partial \sigma_Z$ can be expanded as follows:

$$\begin{aligned} \frac{\partial U}{\partial \sigma_Z} = & \frac{1}{\sqrt{2\pi\sigma_Z^2}} \left[\iint_{D_0} u(d, v) e^{-\frac{(Z-\lambda)^2}{2\sigma_Z^2}} (Z-\lambda) d d d v \right. \\ & \left. - \iint_{D_1} u(d, v) e^{-\frac{(Z-\lambda)^2}{2\sigma_Z^2}} (Z-\lambda) d d d v \right]. \end{aligned} \quad (62)$$

Comparing (62) with the first line of (57), we have

$$\frac{\partial U}{\partial \sigma_Z} = \sigma_Z \frac{\partial^2 U}{\partial \lambda^2}. \quad (63)$$

Combining (59), (61) and (63), we have

$$\frac{d\tilde{U}}{d\sigma_Z} = \left. \frac{\partial U}{\partial \sigma_Z} \right|_{\lambda=\tilde{\lambda}} = \sigma_Z \left. \frac{\partial^2 U}{\partial \lambda^2} \right|_{\lambda=\tilde{\lambda}} > 0. \quad (64)$$

Therefore, $\tilde{U}(\sigma_Z)$ is an increasing function of σ_Z .

ACKNOWLEDGMENT

The authors would like to thank Prof. Huadong Meng with California PATH, University of California, Berkeley, for his fruitful discussions and his supports in our early work.

REFERENCES

- [1] A. Shaout, D. Colella, and S. Awad, "Advanced driver assistance systems-past, present and future," in *Proc. 7th Int. Comput. Eng. Conf. IEEE*, 2011, pp. 72–82.
- [2] A. Vahidi and A. Eskandarian, "Research advances in intelligent collision avoidance and adaptive cruise control," *IEEE Trans. Intell. Transp. Syst.*, vol. 4, no. 3, pp. 143–153, 2003.
- [3] A. Mukhtar, L. Xia, and T. B. Tang, "Vehicle detection techniques for collision avoidance systems: A review," *IEEE Trans. Intell. Transp. Syst.*, vol. 16, no. 5, pp. 2318–2338, 2015.
- [4] D. Lee and H. Yeo, "Real-time rear-end collision-warning system using a multilayer perceptron neural network," *IEEE Trans. Intell. Transp. Syst.*, vol. 17, no. 11, pp. 3087–3097, 2016.
- [5] S. Li, K. Li, R. Rajamani, and J. Wang, "Model predictive multi-objective vehicular adaptive cruise control," *IEEE Trans. Control Syst. Technol.*, vol. 19, no. 3, pp. 556–566, 2011.
- [6] M. I. Skolnik, "Introduction to radar," *Radar handbook*, vol. 2, p. 21, 1962.

$$\frac{\partial U}{\partial \lambda} = \frac{1}{\sqrt{2\pi}\sigma_Z} \left[\iint_{D_0} u(d, v) e^{-\frac{(z-\lambda)^2}{2\sigma_Z^2}} d d v - \iint_{D_1} u(d, v) e^{-\frac{(z-\lambda)^2}{2\sigma_Z^2}} d d v \right]. \quad (56)$$

$$\begin{aligned} \frac{\partial^2 U}{\partial \lambda^2} &= \frac{1}{\sqrt{2\pi}\sigma_Z^3} \left[\iint_{D_0} u(d, v) e^{-\frac{(z-\lambda)^2}{2\sigma_Z^2}} (Z-\lambda) d d v - \iint_{D_1} u(d, v) e^{-\frac{(z-\lambda)^2}{2\sigma_Z^2}} (Z-\lambda) d d v \right] \\ &= \frac{1}{\sqrt{2\pi}\sigma_Z^3} \iint_D u(d, v) e^{-\frac{(z-\lambda)^2}{2\sigma_Z^2}} |Z| d d v - \frac{\lambda}{\sqrt{2\pi}\sigma_Z^3} \left[\iint_{D_0} u(d, v) e^{-\frac{(z-\lambda)^2}{2\sigma_Z^2}} d d v - \iint_{D_1} u(d, v) e^{-\frac{(z-\lambda)^2}{2\sigma_Z^2}} d d v \right] \\ &= \frac{1}{\sqrt{2\pi}\sigma_Z^3} \iint_D u(d, v) e^{-\frac{(z-\lambda)^2}{2\sigma_Z^2}} |Z| d d v - \frac{\lambda}{\sigma_Z^2} \frac{\partial U}{\partial \lambda}. \end{aligned} \quad (57)$$

- [7] H. Rohling and M.-M. Meinecke, "Waveform design principles for automotive radar systems," in *Proc. IEEE 2001 CIE Int. Conf. Radar*, vol. 4, 2001, p. 1.
- [8] M. Kunert, "The EU project MOSARIM: A general overview of project objectives and conducted work," in *Proc. 9th Eur. Radar Conf. (EuRAD)*. IEEE, 2012, pp. 1–5.
- [9] G. M. Brooker, "Mutual interference of millimeter-wave radar systems," *IEEE Trans. Electromagn. Compat.*, vol. 49, no. 1, pp. 170–181, 2007.
- [10] M. Goppelt, H. L. Blocher, and W. Menzel, "Automotive radar – investigation of mutual interference mechanisms," *Adv. Radio Sci.*, vol. 8, pp. 55–60, 2010.
- [11] M. Braun, R. Tanbourgi, and F. K. Jondral, "Co-channel interference limitations of OFDM communication-radar networks," *EURADSIP J. Wireless Commun. Netw.*, vol. 2013, no. 1, p. 207, 2013.
- [12] A. Alhourani, R. J. Evans, S. Kandeepan, B. Moran, and H. Eltom, "Stochastic geometry methods for modeling automotive radar interference," *IEEE Trans. Intell. Transp. Syst.*, vol. 19, no. 2, pp. 1–12, 2018.
- [13] C. Fischer, M. Goppelt, H.-L. Blöcher, and J. Dickmann, "Minimizing interference in automotive radar using digital beamforming," *Adv. Radio Sci.*, vol. 9, no. B. 2, pp. 45–48, 2011.
- [14] S. Sun, "Interference mitigation in automotive radars," 2015.
- [15] P. Papadimitratos, A. De La Fortelle, K. Evensen, R. Brignolo, and S. Cosenza, "Vehicular communication systems: Enabling technologies, applications, and future outlook on intelligent transportation," *IEEE Commun. Mag.*, vol. 47, no. 11, 2009.
- [16] H. Ruan, Y. Liu, H. Meng, and X. Wang, "Sharing for safety: The bandwidth allocation among automotive radars," in *Proc. IEEE Int. Conf. Global Signal Process. (GlobalSIP)*, 2016, pp. 1047–1051.
- [17] J. Khoury, R. Ramanathan, D. McCloskey, R. Smith, and T. Campbell, "RadarMAC: Mitigating radar interference in self-driving cars," in *Proc. IEEE Int. Conf. Sens., Commun. Netw.*, 2016, pp. 1–9.
- [18] C. Aydogdu, G. K. Carvajal, O. Eriksson, H. Hellsten, H. Herbertsson, M. F. Keskin, E. Nilsson, M. Rydström, K. Vanäs, and H. Wymeersch, "Radar interference mitigation for automated driving," *arXiv preprint arXiv:1909.09441*, 2019.
- [19] C. Aydogdu, M. F. Keskin, N. Garcia, H. Wymeersch, and D. W. Bliss, "Radchat: Spectrum sharing for automotive radar interference mitigation," *IEEE Trans. Intell. Transp. Syst.*, pp. 1–14, 2019.
- [20] M. E. Russell, A. Crain, A. Curran, R. A. Campbell, C. A. Drubin, and W. F. Miccioli, "Millimeter-wave radar sensor for automotive intelligent cruise control (ICC)," *IEEE Trans. Microw. Theory Techn.*, vol. 45, no. 12, pp. 2444–2453, 1997.
- [21] J. Hasch, E. Topak, R. Schnabel, T. Zwick, R. Weigel, and C. Waldschmidt, "Millimeter-wave technology for automotive radar sensors in the 77 GHz frequency band," *IEEE Trans. Microw. Theory Techn.*, vol. 60, no. 3, pp. 845–860, 2012.
- [22] Y. L. Sit, G. Li, S. Manchala, H. Afrasiabi, C. Sturm, and U. Lubbert, "BPSK-based MIMO FMCW automotive-radar concept for 3D position measurement," in *Proc. 9th Eur. Radar Conf. (EuRAD)*. IEEE, 2018, pp. 289–292.
- [23] X. Yi, G. Feng, Z. Liang, C. Wang, B. Liu, C. Li, K. Yang, C. C. Boon, and Q. Xue, "A 24/77 GHz dual-band receiver for automotive radar applications," *IEEE Access*, 2019.
- [24] F. Folster, H. Rohling, and U. Lubbert, "An automotive radar network based on 77 GHz FMCW sensors," in *IEEE Int. Radar Conf., 2005*. IEEE, 2005, pp. 871–876.
- [25] H. Forstner, H. Knapp, H. Jager, E. Kolmhofer, J. Platz, F. Starzer, M. Tremel, A. Schinko, G. Birschkus, J. Bock *et al.*, "A 77GHz 4-channel automotive radar transceiver in SiGe," in *2008 IEEE Radio Frequency Integrated Circuits Symp.* IEEE, 2008, pp. 233–236.
- [26] M. Braun *et al.*, "Parametrization of joint OFDM-based radar and communication systems for vehicular applications," in *20th Int. Symp. Pers., Indoor and Mobile Radio Commun.* IEEE, 2009, pp. 3020–3024.
- [27] A. Turlapaty, Y. Jin, and Y. Xu, "Range and velocity estimation of radar targets by weighted OFDM modulation," in *Proc. IEEE Radar Conf.*, 2014, pp. 1358–1362.
- [28] M. R. Bell, "Information theory and radar waveform design," *IEEE Trans. Inf. Theory*, vol. 39, no. 5, pp. 1578–1597, 1993.
- [29] A. Leshem, O. Naparstek, and A. Nehorai, "Information theoretic adaptive radar waveform design for multiple extended targets," *IEEE J. Sel. Topics Signal Process.*, vol. 1, no. 1, pp. 42–55, 2007.
- [30] A. Lenz, M. S. Stein, and A. L. Swindlehurst, "Joint transmit and receive filter optimization for sub-nyquist delay-doppler estimation," *IEEE Trans. Signal Process.*, vol. 66, no. 10, pp. 2542–2556, 2018.
- [31] C. Knapp and G. Carter, "The generalized correlation method for estimation of time delay," *IEEE Trans. Acoust., Speech, Signal Process.*, vol. 24, no. 4, pp. 320–327, 1976.
- [32] C. Chen and P. P. Vaidyanathan, "MIMO radar ambiguity properties and optimization using frequency-hopping waveforms," *IEEE Trans. Signal Process.*, vol. 56, no. 12, pp. 5926–5936, 2008.
- [33] M. Stein, M. Castañeda, A. Mezghani, and J. A. Nosssek, "Information-preserving transformations for signal parameter estimation," *IEEE Signal Process. Lett.*, vol. 21, no. 7, pp. 866–870, 2014.
- [34] P. Heidenreich and A. M. Zoubir, "Fast maximum likelihood DOA estimation in the two-target case with applications to automotive radar," *Signal Process.*, vol. 93, no. 12, pp. 3400–3409, 2013.
- [35] S. M. Kay, *Fundamentals of statistical signal processing*. Prentice Hall PTR, 1993.
- [36] A. G. Stove, "Linear FMCW radar techniques," in *IEE Proc. F (Radar and Signal Process.)*, vol. 139, no. 5. IET, 1992, pp. 343–350.
- [37] E. Hyun, W. Oh, and J. Lee, "Two-step moving target detection algorithm for automotive 77 GHz FMCW radar," in *2010 IEEE 72nd Veh. Technol. Conf - Fall*, 2010, pp. 1–5.
- [38] Y. Hua, "Estimating two-dimensional frequencies by matrix enhancement and matrix pencil," *IEEE Trans. Signal Process.*, vol. 40, no. 9, pp. 2267–2280, 1992.
- [39] F. J. Massey Jr, "The Kolmogorov-Smirnov test for goodness of fit," *J. Amer. Statist. Assoc.*, vol. 46, no. 253, pp. 68–78, 1951.
- [40] K. Lee and H. Peng, "Evaluation of automotive forward collision warning and collision avoidance algorithms," *Veh. Syst. Dynamics*, vol. 43, no. 10, pp. 735–751, 2005.
- [41] M. M. Minderhoud and P. H. Bovy, "Extended time-to-collision measures for road traffic safety assessment," *Accident Anal. & Prevention*, vol. 33, no. 1, pp. 89–97, 2001.
- [42] J. S. Jermakian, S. Bao, M. L. Buonarosa, J. R. Sayer, and C. M. Farmer, "Effects of an integrated collision warning system on teenage driver behavior," *J. of Safety Res.*, vol. 61, pp. 65–75, 2017.
- [43] D. J. Phillips, J. C. Aragon, A. Roychowdhury, R. Madigan, S. Chintakindi, and M. J. Kochenderfer, "Real-time prediction of automotive collision risk from monocular video," *arXiv preprint arXiv:1902.01293*, 2019.
- [44] S. M. Kay, "Fundamentals of statistical signal processing, vol. ii: Detection theory," *Signal Processing. Upper Saddle River, NJ: Prentice Hall*, 1998.
- [45] S. Moon, I. Moon, and K. Yi, "Design, tuning, and evaluation of a full-range adaptive cruise control system with collision avoidance," *Control Eng. Practice*, vol. 17, no. 4, pp. 442–455, 2009.